Pitsilis, G. & Marshall, L. 2006. A trust-enabled P2P recommender system. In Enabling Technologies: Infrastructure for Collaborative Enterprises, 2006. WETICE'06. 15th IEEE International Workshops on (pp. 59-64). IEEE.

Resnick, P. & Varian, H. R. 1997. Recommender systems. Communications of the ACM, 40(3), 56-58.

Resnick, P., Iacovou, N., Suchak, M., Bergstrom, P. & Riedl, J. 1994. GroupLens: an open architecture for collaborative filtering of netnews. In Proceedings of the 1994 ACM conference on Computer supported cooperative work (pp. 175-186). ACM.

Sarda, K., Gupta, P., Mukherjee, D., Padhy, S. & Saran, H. 2008. A distributed trust-based recommendation system on social networks. In 2nd IEEE Workshop on Hot Topics in Web Systems and Technologies (HotWeb 2008). IEEE (December 2008).

Schein, A. I., Popescul, A., Ungar, L. H. & Pennock, D. M. 2002. Methods and metrics for cold-start recommendations. In Proceedings of the 25th annual international ACM SIGIR conference on Research and development in information retrieval (pp. 253-260). ACM.

Smith, M., Milic-Frayling, N., Shneiderman, B., Mendes Rodrigues, E., Leskovec, J. & Dunne, C.2010. NodeXL: a free and open network overview, discovery and exploration add-in for Excel 2007/2010, http://nodexl.codeplex.com/ from the Social Media Research Foundation, http://www.smrfoundation.org

Sun, Y. L., Yu, W., Han, Z. & Liu, K. R. 2006. Information theoretic framework of trust modeling and evaluation for ad hoc networks. Selected Areas in Communications, IEEE Journal on, **24**(2), 305-317.

Tseng, S. & Fogg, B. J. 1999. Credibility and computing technology. Communications of the ACM, **42**(5), 39-44.

Victor, P., Cornelis, C., De Cock, M. & Teredesai, A. 2011. Trust-and distrust-based recommendations for controversial reviews. IEEE Intelligent Systems, **26**(1), 48-55.

Walter, F. E., Battiston, S. & Schweitzer, F. 2008. A model of a trust-based recommendation system on a social network. Autonomous Agents and Multi-Agent Systems, **16**(1), 57-74.

Wang, J., Yin, J., Liu, Y. & Huang, C. 2011. Trust-based collaborative filtering. In Fuzzy Systems and Knowledge Discovery (FSKD), 2011 Eighth International Conference on (Vol. 4, pp. 2650-2654). IEEE.

Weng, J., Miao, C. & Goh, A. 2006. Improving collaborative filtering with trust-based metrics. In Proceedings of the 2006 ACM symposium on Applied computing (pp. 1860-1864). ACM.

Ziegler, C. N. & Golbeck, J. 2007. Investigating interactions of trust and interest similarity. Decision Support Systems, **43**(2), 460-475.

Submitted: 20/03/2013
Revised: 11/02/2014
Accepted: 12/02/2014

Journal of Engg. Research Vol. 2 - (2) June 2014 pp. 49 - 61

تحليل الضغط لمجال المويجات للفتحة الاصطناعية للتداخل السونارية التفاضلية للصور الرادارية (Dinsar)

*راشد حسين و **عبدالرحمن ميمن

* أستاذ مساعد ونائب مدير كلية هندسة العلوم والتكنولوجيا - جامعة همدرد كراتشي
rashid.hussain@handard.edu.pk - باكستان - 74600

** عميد كلية هندسة العلوم والتكنولوجيا - جامعة همدرد كراتشي 74600 - باكستان

الخلاصة

يشرح هذا البحث عن أساليب ضغط الحزمة على أساس العويجات للفتحة الاصطناعية للتداخل السونارية التفاضلية للصور الرادارية (DInSAR). الفتحة الاصطناعية الرادارية (SAR) هي تكنولوجيا تصوير الرادار القمر الصناعي، والتي تستخدم لالتقاط البيانات للفترات المختلفة مثل الليل أو النهار ولمختلف الطقوس، مثل العديد من أوهام الأقمار الصناعية، يمكن ضغط الصور الرادارية (DInSAR) أثناء الاسترجاع، النقل والتخزين، تفتيت الضغط الأمثل مطلوبة للحفاظ على المعلومات المحتوية في الصورة عالية الطيف.

توضح هذه الدراسة تحليل الضغط ما بعد المعاجلة للصور (DInSAR) باستخدام حزم المويجات مع التركيز على انتقاء مناسب للأ... المويجية والمستوى العتبة للأساليب التجريبية.

السلوكيات المختلفة للضغط تسمح لنا بالتصميم واختيار الأم المويجية/ الأساليب العتبة لتحقيق الأداء الأمثل. ولوحظ أن وظائف المويجات سيمليت تملك الأداء المتسق من حيث معنى الخطأي لمربع (MSE) وإشارة الذروة إلى قيم نسبة الضوضاء (PSNR). الأم المويجية bior 3، 7 أظهرت أسواء الأداء. نجح البحث التحقيقي في تقديم الأداء المحسن للضغط من الأم المويجية للصور الرادارية (DInSAR).

الكلمات الرئيسية: الفتحة الصناعية الرادارية، المستوى العتبة للأساليب التجريرية، صورة مضغوطة، صور رادار القمر الصناعي والاستشعار عن بعد.

Wavelet domain compression analysis for differential interferometric synthetic aperture radar (DInSAR) images

RASHID HUSSAIN* AND ABDUL REHMAN MEMON**

* *Assoc. Prof. and Deputy Director, Faculty of Engineering Science and Technology Hamdard University, Karachi 74600, Pakistan. rashid.hussain@hamdard.edu.pk*
** *Dean, Faculty of Engineering Science and Technology, Hamdard University Karachi 74600, Pakistan.*
* *Corresponding Author: rashid.hussain@hamdard.edu*

ABSTRACT

This research expounds on wavelet packet based compression methods for Differential Interferometric Synthetic Aperture Radar (DInSAR) images. Synthetic Aperture Radar (SAR) is a Satellite Radar imaging technology, which is used to capture data for different periods during day or night and at different weather conditions. Like many of the satellite imaginary, (DInSAR) Images can be compressed during retrieval, transmission and storage. Optimal compression techniques are required to preserve the information content of the high spectral image. This study elucidates the post-processing compression analysis of (DInSAR) images, using Wavelet Packets focusing on suitable selection of mother wavelets and empirical thresholding methods. Different behaviors of compression allow us to design and to select the mother wavelets/ threshold methods for optimal performance. It is observed that Symlet wavelet functions had consistent performance in terms, of Mean Square Error (MSE) and Peak Signal to Noise Ratio values (PSNR). Mother wavelet ***bior3.7*** showed worse performance. The research investigation succeeded in providing improved compression performance of various mother wavelets for (DInSAR) images.

Keywords: Synthetic aperture radar (SAR); thresholding methods; compressed image; satellite radar images; remote sensing.

INTRODUCTION

High Spectral Space Borne Satellite Imaginary, such as Synthetic Aperture Radar (SAR) images, can be very beneficial for various ecological and environmental predictions and monitoring. Land sliding, volcanic activities and mine subsidence are some of the examples. Some of the recent researches in SAR include: unsupervised amplitude and texture classification of SAR images with multinomial latent model (Kayabol & Zerubia 2013), SAR-based terrain classification using weakly supervised hierarchical markov aspect models (Yang *et al.*, 2013), optimizing multiscale SSIM for compression via MLDS (Charrier *et al.*, 2013), saliency detection in the compressed domain for adaptive image retargeting (Fang *et al.*, 2013), the imaging of objects under the foliages (Yue *et al.*, 2012), ionosphere total electron content

(TEC) measurement (Jingyi & Zebker 2012), bio-mass imaging in forests structure monitoring (Neumann *et al.*, 2012) and performance analysis of wavelet packet based image compression in the presence of noise (Hussain *et al.*, 2011).

Differential Interferometric Synthetic Aperture Radar (DInSAR) is the latest version of SAR which exploits satellite radar images taken at different sets of angles, polarizations and wavelengths at different times to form digital elevation models. It is used to detect changes occurring between two consecutive data acquisitions. Grabriel *et al.* (1989) used DInSAR to find the changes in the soil moisture, by measuring changes in the penetration depth of the electromagnetic pulses. Massonnet (1993) detected and validated quake signature using European Remote Sensing satellite (ERS-1) data. Recent researches in DInSAR include: the tectonics monitoring of earthquake risk management (Fornaro *et al.*, 2012), measurement of volume change during land deformation (Sumantyo *et al.*, 2012) and accurate soil moisture monitoring of land subsidence (Morrison *et al.*, 2011).

Wavelet Packet belongs to the wavelet transform, in which signal is passed through a higher number of filters than in the discrete wavelet transform (DWT). In wavelet packet decomposition, both detail and approximation coefficients are decomposed to form a full binary tree. Due to the full decomposition it offers greater range of signal analysis and high perceptual image quality with a low bit rate. On the contrary, only previous approximation coefficients are decomposed to form binary tree in discrete wavelet transform (Coifman & Wickerhauser 1992; Daubechies 1992 and Gonzalez & Wood 2002).

Existing literature suggests that wavelet transform has an array of applications. Recent research includes: the wavelet Bayesian network image de-noising (Ho & Hwang 2013), the improved bounds for subband-adaptive iterative shrinkage/ thresholding algorithms (Zhang & Kingsbury 2013), the wavelet domain multifractal analysis for static and dynamic texture classification (Hui Ji *et al.*, 2013), the multiscale image fusion using the undecimated wavelet transform with spectral factorization and nonorthogonal filter banks (Ellmauthaler *et al.*, 2013), the 3D steerable wavelets in practice (Chenouard & Unser 2013) and selecting the best wavelet for texture discrimination (Chaudhry *et al.*, 2007).

Compression scores can be analyzed by the following two parameters: the retained energy *E(%)* and the number of zeros *NZ(%)* (Misiti *et al.*, 2008). The retained energy measures the information retained after the compression, thus it relates with the quality of the compressed image. The number of zeros is another way of measuring compression.

Mathematically the retained energy E(%) is defined as (1):

$$E(\%) = 100 \times \left(\frac{\|C\|}{\|C\|} \right)^2 \quad (1)$$

Where C is the coefficients of the original signal, CC are the coefficients of the current decomposition, and $\|.\|$, the vector norm.

Mathematically the number of zeros $NZ\ (\%)$ is defined as (2):

$$NZ(\%) = 100 \times \left(\frac{\text{Number of zeros of the decomposition}}{\text{Number of coefficients}} \right) \tag{2}$$

Key criterion is the quality of the compressed image which is obtained through mean square error (MSE) and peak signal noise ratio (PSNR). MSE is a quality assessment method, used to measure the deformation of the image. It can be expressed as the mean of square distance between pixel of the original image A_{ij} and pixel of the reconstructed image B_{ij}, Mathematically it can be given as (3):

$$MSE = \sum_{i=1}^{x} \sum_{j=1}^{y} \frac{\left(\left| A_{ij} - B_{j} \right| \right)^2}{x * y} \tag{3}$$

The smaller value of MSE results in large value of the PSNR means that reconstructed image is close to the original image. Mathematically it can be given as (4):

$$PSNR = 10 \ \log^* \left(\frac{255^2}{MSE} \right) \tag{4}$$

The motivation of this study is to reduce redundancy and preserve vital information content of compressed DInSAR Images. This study expounded on wavelet packet based compression for SAR images with focus on selecting appropriate mother wavelet for image compression.

PROCEDURE

Wavelet based implementation involves various components for compression analysis including wavelet transformation, thresholding, entropy encoding and non-zero coefficient selection (Gonzalez & Wood 2002) as shown in figure 1. Wavelet transformations involve converting signal/image into coefficients across various sub-bands. The thresholding criterion involves the selection of coefficient for signal/image reconstruction. Global and level dependents are the two choices for thresholding. In global thresholding a single value of the thresholding is applied across each sub-band of the image, while in level dependent thresholding different values of the thresholding are applied across each sub-band of the image. Therefore if the noise is independent of the sub-band, then global thresholding could produce optimal results; while, if noise model varies across different sub-bands, then level dependent thresholding could

possibly produce optimal results (Donoho & Johnstone 1994). Mathematically it can be given as (5):

$$\lambda_{Global} = \sqrt{2 \ln N}\sigma \tag{5}$$

Where N being the signal length, σ being the noise variance.

It could be further defined in terms of soft and hard thresholding. Entropy coding used more frequent short code words first for assigning more encoded values; recursively these short code words were utilized to encode longer code words for assigning less encoded values. In this way, information (an image in our case) can be

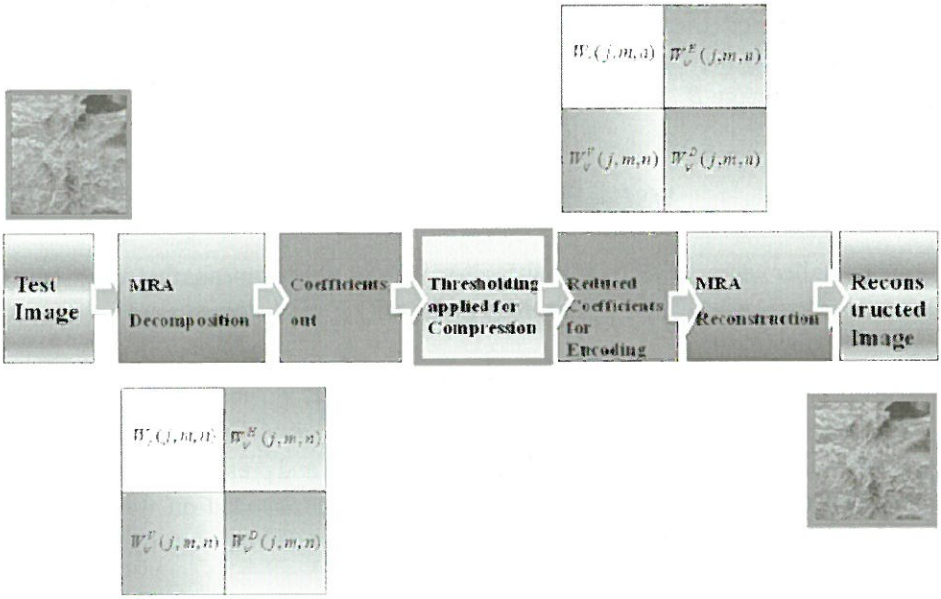

Fig. 1. Wavelet transform based compression analysis for DInSAR Images.

The procedure describes compression performance analysis of mother wavelets for DInSAR Images involve the following steps:

1 - Three DInSAR Images were selected for compression performance analysis. The first image is gray image *dinsar1* with 256x256 pixels. The second image is color image *dinsar2* with 256x256 pixels. The third image is colored image *dinsar3* with 320x400 pixels.

2 - Wavelet transformation involves the conversion of image into large number of coefficients. This process is termed as multi resolution decomposition analysis (Gonzalez & Wood 2002).

3 - Thresholding methods for compression govern the criteria for selecting

coefficients. Three empirical methods were used for thresholding, namely *Balance Sparsity-norm, Removing near zero* and *Balance Sparsity-norm (sqrt)*. Details can be found in (Misiti *et al.*, 2008). For *Balance Sparsity-norm, c* denotes the detail coefficients; two curves are built associating, for each possible threshold value *t*, two percentages:

- The 2-norm recovery in percentage.
- The relative sparsity in percentage, obtained from compressed image by setting to zero the coefficients less then t in absolute value.

A default is provided by taking the square root of the previous *t*.

For *Remove Near 0 c* denotes the detail coefficients at level 1obtained from the decomposition of the image using *db1*. The threshold value is set to median (abs(c)) or to 0.05 max (abs(c)) if median(abs(c)) = 0.

If the detail coefficients c of the signal/image are very small, then they can be suppressed to zero without compromising the quality of the image. The value of detail coefficients c is governed by threshold t. High value of threshold t may result in reduction of detail coefficients which result in loss of energy (information content). Compression rate and energy retention can be governed by threshold t and detail coefficients c of the signal/image.

4 - Entropy coding responsible for further compressing the quantized values containing redundancies in the given set of data.

5 - Wavelet inverse transformation involves the conversion of entropy encoded coefficients to the compressed image. This process is termed as multi resolution reconstruction analysis (Gonzalez & Wood 2002).

6 - Compression performance of various thresholding methods involves *global threshold, Retained Energy (%)* and *Number of Zeros (%)*.

7 - Compression performances of various mother wavelets are measured using Peak Signal to Noise Ratio (PSNR) and Mean Square Error (MSE).

8 - Rate-distortion theory provides the foundations for lossy data/image compression. The Rate R defines the minimum number of bits per symbol to approximately reconstruct the image without exceeding a given distortion D. Mathematically Rate-distortion function can be given as (6):

$$R(D) = \frac{1}{2}\log_2\left(\frac{\sigma^2{}_x}{D}\right) \tag{6}$$

Where $\sigma^2{}_x$ is the variance of signal/image x, this study applied MSE as the measure of distortion D.

The Matlab ® based analysis has been performed on DInSAR Images, as shown in figure 2(a) as *dinsar1*, figure 2(b) as *dinsar2* and figure 2(c) as *dinsar3*. Test images consist of both grey and color images with different dimensions. In SAR images, radar waves used three polarizations namely HH-pol, VV-pol and VH-pol in image synthesized as in case of images *dinsar2* and *dinsar3*.

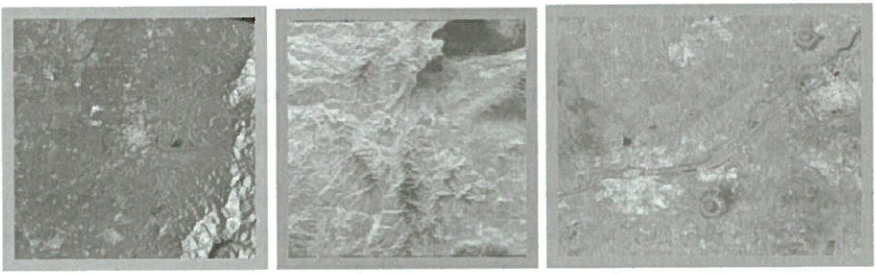

(a) (b) (c)

Fig. 2. Test images consists of both grey and color images with different dimensions.

RESULTS AND DISCUSSION

This research focuses on the properties of mother wavelets that lead to the best performance for DInSAR Image compression. These findings are applicable for efficient compression coding. DInSAR image compression was performed for various simulation settings. Results have established the performance of wavelet packet compression for thresholding namely *Balance Sparsity-norm, Removing near zero* and *Balance Sparsity-norm (sqrt)*; further details can be seen at (Misiti *et al.*, 2008). These finding are applicable to many problems that involve the mother wavelet. Here, we have used them in the framework of wavelet thresholding (Donoho & Johnstone 1994), for a well known application of image reconstruction.

Performance Design Criterion

The performance design criterion focuses mother wavelet properties including compactly supported symmetry, orthogonality and vanishing moments. Mother wavelet involves the selection of appropriate wavelet function translation and dilation.

$$\psi_{s,\tau}(t) = \frac{1}{\sqrt{|s|}} \psi\left(\frac{t-\tau}{s}\right) \tag{7}$$

Equation (7) represents Mother wavelet prototype, where (τ, s) are translation and scale respectively (Cohen *et al.*, 1991). Translation of the wavelet defines the

location of the window, while $\frac{1}{\sqrt{|s|}}$ is used for wavelet normalization and $\psi\left(\frac{t-\tau}{s}\right)$ is the mother wavelet (Cohen *et al.*, 1991).

Various mother wavelets will demonstrate in this analysis including *Symlet* (Daubechies 1992), *Coiflet* (Beylkin *et al.*, 1991) and *Bior* (Cohen *et al.*, 1991). Mother wavelet *Daubechies* belongs to compactly supported orthogonal wavelets. Mathematically, it is represented as *dbN*, where *N* is the order, and db represents *Daubechies* wavelet. *db1* and *db2* are used in this study. Mother wavelet *Bior* has linear phase property. Four *biorN* family members are used in this study (*bior3.7,bior 4.4, bior 5.5 and bior 6.8*). Three *coifletN* family members are used in this study (*coif1,coif2 and coif4*). Coiflet wavelet is more symmetrical than *db* wavelet. Coiflet wavelet belongs to family of near-symmetrical wavelets. Symlet wavelets belong to *Daubechies* wavelet with increased symmetry. Four *symlet* family members are used in this study (*sym3,sym4, sym5 and sym6*).

Three empirical methods are analyzed in terms of percentage of energy retained and percentage of number of zero for image global threshold, as shown in table 1, table 2 and table 3. A significant reduction percentage of number of zero is observed in *Removing near zero* method, compared to *Balance Sparsity-norm* method for given test images.

Table 1. Compression performance of various thresholding methods (dinsar1256 x256)

Threshold Method	Global Threshold	Retained Energy (%)	Number of Zeros (%)
Balance Sparsity-norm	148.4	93.23	93.24
Removing near zero	8.5	99.92	**44.45**
Balance Sparsity-norm (sqrt)	12.18	99.83	54.34

Table 2. Compression performance of various thresholding methods (dinsar2 256x256)

Threshold Method	Global Threshold	Retained Energy (%)	Number of Zeros (%)
Balance Sparsity-norm	248.8	94.78	94.74
Removing near zero	0.5	100.00	**11.18**
Balance Sparsity-norm (sqrt)	15.77	99.82	73.02

Table 3. Compression performance of various thresholding methods (dinsar3 320x400)

Threshold Method	Global Threshold	Retained Energy (%)	Number of Zeros (%)
Balance Sparsity-norm	404.5	94.34	94.34
Removing near zero	5	99.98	**50.02**
Balance Sparsity-norm (sqrt)	20.11	99.70	84.53

Compression Performance of Various Mother Wavelets (*dinsar1* 256x256) is shown in Table 4.

Starting with Daubechies wavelet functions *db1*; the image quality index Peak Signal to Noise Ratio (PSNR) is 48.6649 with Mean Square Error (MSE) of 0.8912. For Daubechies wavelet functions *db2*, the image quality index Peak Signal to Noise Ratio (PSNR) is 48.0893 Mean Square Error (MSE) of 1.0175. It is found that for *db2* Mean Square Error (MSE) value increases compared with *db1*.

For Coiflet wavelet functions *Coif1*, *Coif2* and *Coif4*, the image quality index Peak Signal to Noise Ratio (PSNR) is 48.07 with Mean Square Error (MSE) of 1.02.

Another set of analysis includes bi-orthogonal wavelet functions; *bior1.5*, *bior3.7*, *bior4.4*, *bior5.5* and *bior6.8*. For bi-orthogonal wavelet functions *bior1.5*, the image quality index Peak Signal to Noise Ratio (PSNR) is 48.1838 with Mean Square Error (MSE) of 0.9956. For bi-orthogonal wavelet functions *bior3.7*, the image quality index Peak Signal to Noise Ratio (PSNR) is **44.2305** with Mean Square Error (MSE) of **2.4742**. It is concluded that mother wavelet *bior3.7* showed worse results in terms of Mean Square Error (MSE) and Peak Signal to Noise Ratio values (PSNR).

Another set of analysis includes Symlet wavelet functions; *sym3*, *sym4*, *sym5* and *sym6*. It is observed that Symlet wavelet functions have consistent performance in terms of Mean Square Error (MSE) and Peak Signal to Noise Ratio values (PSNR). Optimal DInSAR images obtained by wavelet packed based compression using *sym3* is shown in table 4.

Last set of analysis includes rate-distortion based R (*D*) function applied on compressed image in the wavelet packet domain. For most of wavelet functions, consistent performance is observed in terms of rate-distortion criterion. Optimal value is obtained using *sym3* as shown in table 4.

Table 4. Compression performance of various mother wavelets (*dinsar1 256x256*)

Mother Wavelets	MSE	PSNR	R(D)
db:1	0.8912	48.6649	1.59
db:2	1.0175	48.0893	1.53
Coif:1	1.0200	48.0786	1.52
Coif:2	1.0235	48.0639	1.51
Coif:4	1.0116	48.1149	1.53
Bior:1.5	0.9956	48.1838	1.54
Bior:3.7	**2.4742**	**44.2305**	**1.08**
Bior:4.4	1.0670	47.8831	1.51
Bior:5.5	0.9588	48.3477	1.60
Bior:6.8	1.0747	47.8519	1.50
Sym:3	1.0124	48.1113	1.53
Sym:4	1.0125	48.1109	1.53
Sym:5	1.0162	48.0951	1.52
Sym:6	1.0086	48.1277	1.54

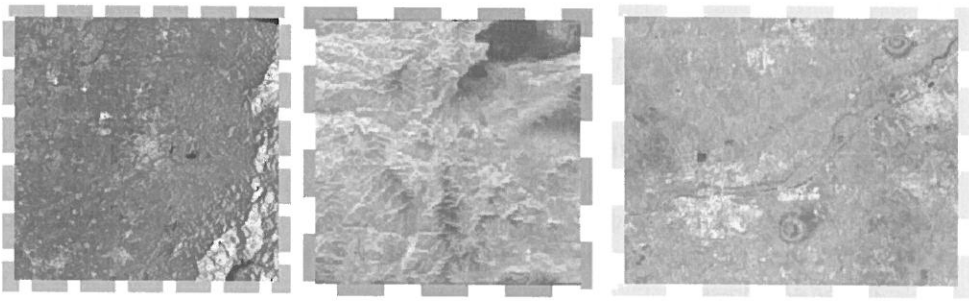

(a) (b) (c)

Fig. 3. Compressed DInSAR Images using *sym3* mother wavelet

CONCLUSION

In this study, an investigation has been made on wavelet packet compression for Differential Interferometric Synthetic Aperture Radar (DInSAR) Images. Due to the high spectral nature of the images, the selection of mother wavelets and threshold methods may vary. This paper is an attempt to introduce a framework for an efficient selection of mother wavelets and threshold methods for (DInSAR) Image compression. Some of the research challenges are region of interest based compression, ground moving target imaging and three dimensional SAR image processing.

In Summary:

1 - During the investigation of mother wavelets and threshold methods for (DInSAR) Image compression, it was noticed that mother wavelets demonstrated consistent performance except *bior3.7* which did not yield optimal results.

2 - We applied image quality matrix Mean Square Error (MSE) and Peak Signal to Noise Ratio values (PSNR) to DInSAR Images. The image quality assessment is obtained by calculating the ratio between original image and compressed image. This measure involves the pixel value of corresponding two images.

3 - It is observed that Symlet wavelet functions have consistent performance in terms of Mean Square Error (MSE) and Peak Signal to Noise Ratio (PSNR) values.

Optimal DInSAR images obtained by wavelet packed based compression using *sym3* can be seen in table 4.

Rate-distortion criterion also demonstrated mother wavelet *sym3* as a best choice.

DInSAR images after compression can be seen in figure 3.

4 - A significant reduction percentage of number of zero is observed in *Removing near zero* method, compared to *Balance Sparsity-norm* method for DInSAR images.

5 - Recently, various studies have been conducted for the appropriate selection of mother wavelets for image reconstruction. As far as DInSAR image is concerned, limited studies have been carried out. In future, more research could be conducted for the selection of appropriate mother wavelet for SAR Image compression.

ACKNOWLEDGMENTS

We would like to thank Gilbert Strang, Mallat S.G., Rafael Gonzalez and David Donoho for providing theoretical framework for wavelet in image processing. We also would like to thank Matthew R. Lopez from Sandia National Laboratories Albuquerque, NM, USA, Ellen O'Leary from Radar Data Center, Jet Propulsion Laboratory Pasadena, CA, Yen, J. from National Donghwa University, Institute of Earth Sciences Taiwan for facilitating SAR resources and images. We also wish to thank M. Misiti, Y. Misiti from The MathWorks, Inc for facilitating Matlab based implementation of wavelet and to the Graduate School of Engineering Sciences and Information Technology, Hamdard University for their logistic support and services.

REFERENCES

Beylkin, G., Coifman, R. & Rokhlin, V. 1991. Fast wavelet transforms and numerical algorithms, Communications on Pure and Applied Mathematics, **44**: 141-183.

Chenouard, N. & Unser, M. 2013. 3D Steerable wavelets in practice, IEEE Transactions on Image Processing **21**(11): 4522-4523.

Chaudhry, M., Jafri, A. M. N., Mufti, M. & Akbar, M. 2007. Design of appropriate wavelet bases for texture discrimination, Kuwait Journal of Science and Engineering **34**(2): 73-84

Charrier, C., Knoblauch, K., Maloney, L. T., Bovik, A. C. & Moorthy, A. K. 2013. Optimizing multiscale SSIM for compression via MLDS, IEEE Transactions on Image Processing **21**(12): 4682-4694.

Coifman, R. R. & Wickerhauser, M. V. 1992. Entropy-based algorithms for best basis selection, IEEE Transactions on Information Theory, **38**(2).

Cohen, A., Daubechies, I. & Feauveau, J. C. 1991. Biorthogonal bases of compactly supported wavelets, Communications on Pure and Applied Mathematics, **45**(5): 485-560.

Daubechies, I. 1992. Ten lectures on wavelets. Society of Industrial and Applied Mathematics, Soc. for Ind. & Appl. Math.198: 254-257, 1st ed.

Donoho, D. L. & Johnstone, I. M. 1994. Ideal sp. adaptation. via wavelet shrinkage. Biometrika, **81**(3):425-455.

Ellmauthaler, A., Pagliari, C. L. & da Silva, E. A. B. 2013. Multiscale image fusion using the undecimated wavelet transform with spectral factorization and nonorthogonal filter banks, IEEE Transactions on Image Processing **22**(3): 1005-1017.

Fang, Y., Chen, Z., Lin, W. & Lin, C. W. 2013. Saliency detection in the compressed domain for adaptive image retargeting, IEEE Transactions on Image Processing 21(9): 3888-3901.

Fornaro, G., Atzori, S., Calo, F., Reale, D. & Salvi, S. 2012. Inversion of wrapped differential interferometric SAR Data for fault dislocation modeling, Geoscience and Remote Sensing, IEEE Transactions on Image Processing **50**(6): 2175-2184.

Gonzalez, R. & Wood, R. 2002. Digital image processing, Pearson Education, Inc., 2nd edition.

Grabriel, A. K., Goldstein, R. & Zebker, H. A. 1989. Mapping small elevation changes over large areas: Differential radar interferometry, Journal of Geophysical Research, **94**: 9183-9191.

Ho, J. & Hwang, W. L. 2013. Wavelet bayesian network image de-noising, IEEE Transactions on Image Processing **22**(4): 1277–1290.

Hui, Ji., Xiong, Yang., Haibin, Ling. & Yong, Xu. 2013. Wavelet domain multifractal analysis for static and dynamic texture classification, IEEE Transactions on Image Processing **22**(1): 286-299.

Hussain R., Sikander M. A., Sheeraz A. , Memon A.R., 2011. Performance Analysis of Wavelet Packet Based Image compression in the Presence of Noise Patterns. Int'l Jour. of Acad. Research **3**(2):

Jingyi, Chen & Zebker, H. A. 2012. Ionospheric artifacts in simultaneous l-band InSAR and GPS observations, Geoscience and Remote Sensing, IEEE Transactions on Image Processing **50**(4): 1227-1239.

Kayabol, K. & Zerubia, J. 2013. Unsupervised amplitude and texture classification of sar images with multinomial latent model, IEEE Transactions on Image Processing **22**(2): 561-572.

Massonnet, D., Rossi, M., Carmona, C., Adragna, F., Peltzer, G., Fiegl, K. & Rabaute, T. 1993. The displacement field of the Landers earthquake mapped by radar interferometry, Nature. Res., **364**:138-142.

Morrison, K., Bennett, J. C., Nolan, M. & Menon, R. 2011. Laboratory measurement of the DInSAR response to spatiotemporal variations in soil moisture, Geoscience and Remote Sensing, IEEE Transactions on Image Processing **49**(10): 3815 - 3823.

Misiti, M., Misiti, Y., Oppenheim, G. & Poggi, J. M. 2008. Wavelet toolbox 4 - Users's guide, The Math Works, Inc., 2008

Neumann, M., Saatchi, S. S., Ulander, L. M. H. & Fransson, J. E. S. 2012. Assessing performance of L- and P-Band polarimetric interferometric SAR data in estimating boreal forest above-ground niomass, Geoscience and Remote Sensing, IEEE Transactions on Image Processing **50**(3): 714-726.

Sumantyo Tetuko Sri, J. Shimada, M. ; Mathieu, P. ; Abidin, H.Z. 2012. Long-Term Consecutive DInSAR for Volume Change Estimation of Land Deformation, IEEE Transactions on Geoscience and Remote Sensing **50**(1): 259-270

Yang, W., Dai, D., Triggs, B. & Xia, G. S. 2013. SAR-Based terrain classification using weakly aupervised hierarchical Markov aspect models, IEEE Transactions on Image Processing **21**(9): 4232-4243.

Yue, Huang., Ferro-Famil, L. & Reigber, A. 2012. Under-foliage object imaging using

using SAR tomography and polarimetric spectral estimators, IEEE transactions on geoscience and remote sensing **50**(6): 2213-2225.

Zhang, Y. & Kingsbury, N. 2013. Improved bounds for subband-adaptive iterative shrinkage/thresholding algorithms , IEEE Transactions on Image Processing **22**(4): 1373-1381.

Submitted: 29/04/2013
Revised: 07/12/2013
Accepted: 21/12/2013